FEMS Microbiology Ecology, 93, 2017, fix018

doi: 10.1093/femsec/fix018
Advance Access Publication Date: 18 February 2017
Research Article

RESEARCH ARTICLE

Photoacclimation by Arctic cryoconite phototrophs

Rupert G. Perkins[1,*], Elizabeth Bagshaw[1], Lisa Mol[2], Christopher J. Williamson[3], Dan Fagan[3], Maggie Gamble[3] and Marian L. Yallop[3]

[1]Cold Climate Research, School of Earth and Ocean Sciences, Cardiff University, Park Place, Cardiff CF10 3AT, UK, [2]Department of Geography and Environmental Management, UWE Bristol, Coldharbour Lane, Bristol BS16 1QY, UK and [3]School of Biological Sciences, Life Sciences Building, University of Bristol, 24 Tyndall Avenue, Bristol BS8 1TQ, UK

*Corresponding author: Cold Climate Research, School of Earth and Ocean Sciences, Cardiff University, Park Place, Cardiff CF10 3AT, UK. Tel.: +0044 (0)2920 875026; E-mail: PerkinsR@cf.ac.uk

One sentence summary: Ice sheet cryoconite phototrophs utilise a complex mixture of behaviour and physiological downregulation to survive productively in this extreme environment.

Editor: Gary King

Downloaded from https://academic.oup.com/femsec/article/93/5/fix018/3003318 by guest on 20 April 2024

ABSTRACT

Cryoconite is a matrix of sediment, biogenic polymer and a microbial community that resides on glacier surfaces. The phototrophic component of this community is well adapted to this extreme environment, including high light stress. Photoacclimation of the cryoconite phototrophic community on Longyearbreen, Svalbard, was investigated using *in situ* variable chlorophyll fluorescence. Rapid light curves (RLCs) and induction–recovery curves were used to analyse photosystem II quantum efficiency, relative electron transport rate and forms of downregulation including non-photochemical quenching (NPQ) and state transitions in cyanobacteria. Phototrophs used a combination of behavioural and physiological photochemical downregulation. Behavioural downregulation is hypothesised to incorporate chloroplast movement and cell or filament positioning within the sediment matrix in order to shade from high light, which resulted in a lack of saturation of RLCs and hence overestimation of productivity. Physiological downregulation likely consisted of biphasic NPQ, comprising a steadily induced light-dependent form and a light-independent NPQ that was not reversed with decreasing light intensity. State transitions by cyanobacteria were the most likely physiological downregulation employed by cyanobacteria within the mixed phototroph community. These findings demonstrate that cryoconite phototrophs combine multiple forms of physiological and behavioural downregulation to optimise light exposure and maximise photosynthetic productivity. This plasticity of photoacclimation enables them to survive productively in the high-light stress environment on the ice surface.

Keywords: cryoconite; photoacclimation; downregulation; non-photochemical quenching; productivity; fluorescence

INTRODUCTION

Cryoconite (cryo = ice, conite = dust) is an important component of the glacier ecosystem. It consists of debris deposited on the ice surface by wind, water or rockfall from valley sides, and collects in water-filled pools on the surface known as cryoconite holes. The debris contains microorganisms, including photoautotrophs, which contribute to the accumulation of carbon and bioavailable nutrients on glacier surfaces (Hodson *et al.* 2007; Cook *et al.* 2012; Bagshaw *et al.* 2016a). These nutrients are periodically exported to downstream environments via

Received: 20 October 2016; **Accepted:** 16 February 2017
© FEMS 2017. All rights reserved. For permissions, please e-mail: journals.permissions@oup.com

glacier runoff (Bagshaw *et al.* 2010; Lawson *et al.* 2014), and can support biological activity in proximal ecosystems (Foreman, Wolf and Priscu 2004; Bagshaw *et al.* 2013). Microorganisms in cryoconite are typically sourced from the surrounding environments, and include cyanobacteria, microalgae, archaea, bacteria, fungi and heterotrophic protists (Cameron, Hodson and Osborn 2012; Edwards *et al.* 2014; Zawierucha *et al.* 2015; Kaczmarek *et al.* 2016). It is well established that the photosynthetic organisms are active throughout the ablation season, but the mechanisms by which they undertake primary production on the harsh environment of the glacier surface are poorly understood. In this paper, we use *in situ* variable chlorophyll fluorescence to investigate cryoconite community photophysiology in order to gain insight into their adaptation to high light intensity, 24 h photoperiods (and hence the resulting high photodose) and rapid light intensity fluctuation.

Glacier surface microorganisms have been demonstrated to impact on ice surface albedo (Takeuchi 2002b; Yallop *et al.* 2012; Musilova *et al.* 2016), via a phenomenon known as 'biological darkening' (Benning *et al.* 2014; Tedesco *et al.* 2016). *In situ* and *ex situ* studies have demonstrated that this occurs via two mechanisms: production of organic matter, which has a net darkening impact on the sediment (Takeuchi 2002a; Musilova *et al.* 2016), and production of dark pigments (Yallop *et al.* 2012; Lutz *et al.* 2014; Remias *et al.* 2016), which serve to protect photosynthetic apparatus from high light and/or UV (Dieser, Greenwood and Foreman 2010). Yallop *et al.* (2012) demonstrated that highly pigmented populations of algae are widespread in marginal zones of the Greenland ice sheet, both concentrated in cryoconite and living directly on the ice surface. Within cryoconite holes, the material aggregates into granules, forming a matrix of sediment particles and the microbial community, bound with biogenic extracellular polymers (EPS) (Hodson *et al.* 2010; Langford *et al.* 2010; Zarsky *et al.* 2013). These tightly-knit granules give structure to the cryoconite community, with heterotrophic organisms concentrated in the centre and phototrophs around the outside, which promotes community stability on the constantly changing glacier surface. During the summer months, cryoconite is regularly redistributed by flowing meltwater (Irvine-Fynn, Bridge and Hodson 2011); hence, granule formation may be an adaptation to promote community longevity (Bagshaw *et al.* 2016b).

To our knowledge, there have been very limited *in situ* measurements of microbial phototrophs in ice/snow-associated communities, presumably due to the difficulty in collecting data in these harsh environments. McMinn *et al.* (2007) used variable chlorophyll fluorescence to perform measurements on *ex situ* samples of Antarctic sea ice algae. Stibal *et al.* (2007) used *in situ* variable chlorophyll fluorescence to measure snow algae; however, these samples were thawed and analysed in a cuvette system. Yallop *et al.* (2012) investigated ice algal photophysiology and their role in reducing ice sheet albedo, but samples were analysed *ex situ* after thawing. Bagshaw *et al.* (2016b) made a comparative study of Arctic and Antarctic cryoconite using combined oxymetry and fluorescence, also on *ex situ* cryoconite material in a cuvette system. By contrast, this is the first study of cryoconite phototroph photophysiology *in situ*. We use a Walz Water Pulse Amplitude Modulated (PAM) flourometer with fibre optic emitter detector to perform *in situ* rapid light response curves and induction–recovery curves in cryoconite holes on Longyearbreen, Svalbard, in order to understand the role of photophysiological downregulation in optimising primary production in this extreme environment.

METHODS

In situ field measurements and sampling

Field work was carried out at Longyearbreen, Svalbard (78° 10 49 N, 15°30 21 E), in the high-Arctic, on 25–30 August 2015. Longyearbreen is a small (2.5 km^2), thin (53m, Langford *et al.* 2014), predominantly cold-based valley glacier, adjacent to the town of Longyearbyen, surrounded by Tertiary and Cretaceous sandstone (Larsson 1982) interbedded with coal-bearing shales and siltstones (Langford *et al.* 2014). Field observations indicate that sediment production is driven by frost shattering of the bedrock and glacial action. This material is moved onto the glacier surface through aeolian deposition and high frequency rock falls (Etzelmüller *et al.* 2011).

Sampling was undertaken near the centre line of the glacier (Fig. 1), which had relatively high debris concentrations including a small morainic deposit. Three hydrologically connected cryoconite holes were chosen at random within 10 m^2 at 78°10.903 N, 15°31.469 E, for *in situ* measurements and sample collection for identification of the photosynthetic community structure using microscopy and pigment analysis. Sediment depth was 4–6 mm and water depth was 10–15 mm in the three holes.

Bulk samples of cryoconite from each hole were collected immediately after fluorescence measurements were made (see below), using new nitrile gloves and Whirlpak sterile sampling bags (Fisher Scientific). They were frozen within 4 h of collection, and transported frozen in insulated boxes to Cardiff University, UK. Samples for initial microscopy were scraped from the debris or ice surface using an ethanol-sterilised knife or spatula, and transferred to new centrifuge tubes. They were returned to the field laboratory, kept cool and examined within 48 h. During the short sampling period, incoming photosynthetically available radiation (PAR) and water temperature of an example cryoconite hole in the sampling area were monitored using an Apogee Quantum sensor and Campbell Scientific 107 probe, powered by a Campbell Scientific CR10X datalogger.

In situ variable chlorophyll fluorescence measurements were made using a Walz Water PAM fluorometer equipped with a blue light fibre-optic emitter/detector unit. This instrument measures emitted fluorescence yield for calculation of photosystem II quantum efficiency, which in turn can be used to calculate relative electron transport rate as a proxy for photophysiological productivity. Measurements consisted of 10 rapid light curves (RLCs) and 5 induction–recovery curves within each cryoconite hole, carried out over the same time period each day, between approximately 10:00 and 18:00 when solar irradiance was high. The photoperiod at the time of sampling in August 2015 was 20 h. Initially three measurements of RLCs were made with a blue or a red light emitter/detector unit to investigate the relative excitation of microalgae and cyanobacteria, respectively (this was prior to identification of taxa present, however cyanobacteria were expected based on previous work and literature). However, no significant difference was observed between the two systems and therefore measurements were only made with one, the blue light emitter/detector unit. RLCs were in two forms: increasing and decreasing incremental light steps, with five replicates of each, following the methods of Perkins *et al.* (2006). Increasing and decreasing light curves were carried out on separate samples each time and with sequentially increasing or decreasing light levels steps, respectively. Increasing eight-step RLCs were carried out using 30 s incremental light steps between 0 and 3600 μmol m^{-2} s^{-1} PAR. A 600 ms saturating pulse at intensity

Downloaded from https://academic.oup.com/femsec/article/93/5/fix018/3003318 by guest on 20 April 2024

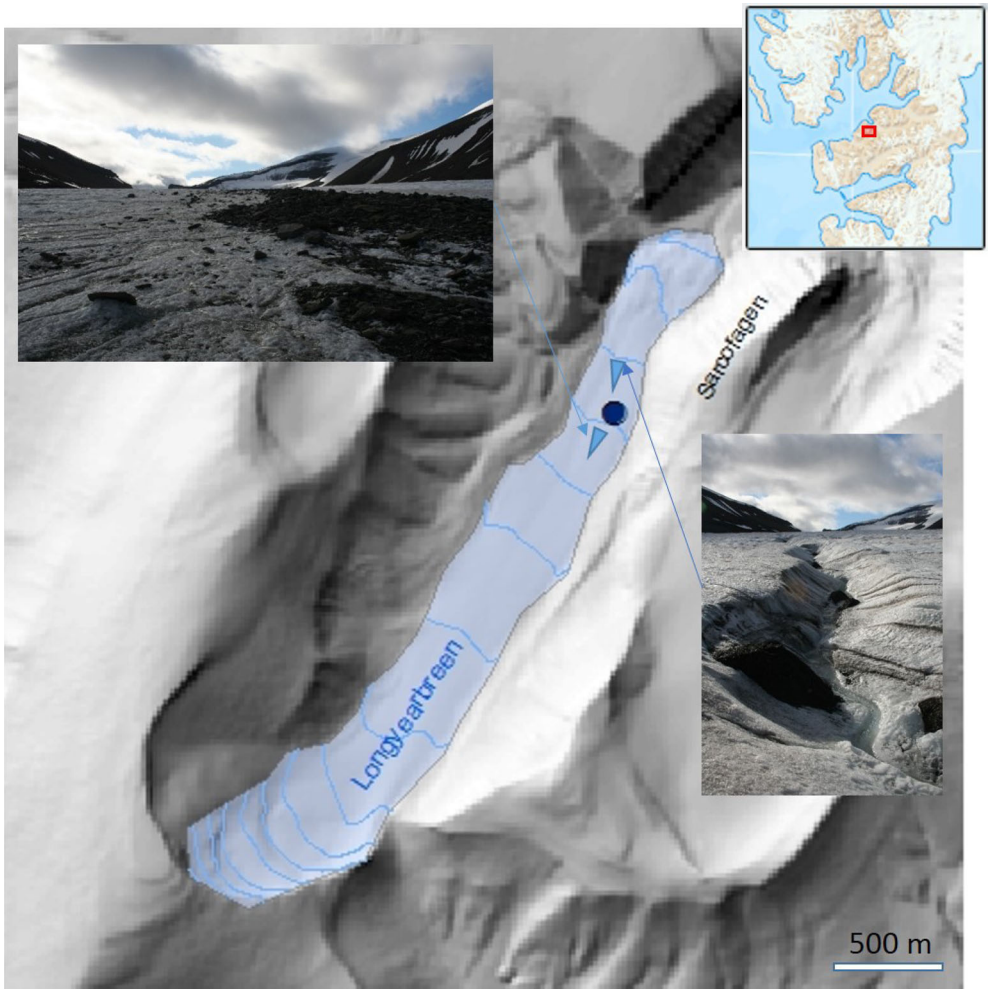

Figure 1. Location of sampling and *in situ* fluorescence measurements (blue dot) on the surface of Longyearbreen, Spitsbergen, Svalbard. Samples were collected from clean ice with intermittent cryoconite coverage, away from adjacent to areas with high concentrations of surface debris (upper insert, lower blue triangle) and meltwater channels (lower insert, upper blue triangle).

setting 10 (in excess of 8000 μmol m^{-2} s^{-1} PAR) was observed to induce full light saturation and rise to maximum fluorescence yield (F_m or F_m'). The increasing incremental light curves were randomly interspersed with five replicates of decreasing incremental light curves. For these light curves, instead of using the pre-programmed RLC settings of the fluorometer, manual light curves were performed, decreasing the light intensity each step using Walz WinControl V3.14 software. At the end of each light curve step, a saturating pulse was performed and the light level reduced to the next lower intensity, culminating in a 30 s dark period measurement. RLCs of relative electron transport rate (rETR) as a function of incremental light intensity were plotted, with rETR calculated as

$$\text{rETR} = \text{quantum efficiency}\,(\Delta F / F_m') \text{ x PAR}/2$$

where $\Delta F/F_m$' is the quantum efficiency calculated as (F_m'-F)/F_m' and where F is the operational fluorescence yield and F_m' is the maximum fluorescence yield in the light and $\Delta F = F_m' - F$. RLC data were analysed by iterative curve fitting of the Eilers and Peeters (1988) model using Sigmaplot V10 statistical software. Light curves data were solved to determine the RLC parameters of relative maximum electron transport rate (rETR_{max}), light utilisation coefficient (α) and light saturation coefficients (E_s and E_k). Light curve coefficients a, b and c and the regression fit for the light curves were all observed to be significant at $p < 0.001$ ensuring accuracy in calculation of the light curve parameters (Perkins *et al.* 2006). Parameters rETR_{max}, α, Ek and Es were analysed for equal variance and normality using the Levene's and Shapiro Wilkes tests respectively in PAST statistical software (Hammer, Harper and Ryan 2001). Data were homoscadestistic and parametric; two factor ANOVA was used to determine significant differences between the three cryoconite holes and between increasing and decreasing RLCs. RLC *in situ* measurements were performed randomly between the three cryoconite holes over 2 days, with induction–recovery curves performed the following day. Again, five sets of measurements were performed for each cryoconite hole. Induction–recovery curves consisted of an initial dark measurement (30 s of darkness) of quantum efficiency (F_v/F_m), followed by a 400 s induction phase of applied actinic light at 803 μmol m^{-2} s^{-1} PAR, with repeated recording of quantum efficiency ($\Delta F/F_m$'). This was then followed by the recovery phase of a further 900 s of darkness, with repeated measurement of quantum efficiency (F_v/F_m). Changes in quantum yield and fluorescence yields (operational fluorescence yield F, and maximum fluorescence yields F_m and F_m') were analysed over the full induction–recovery period.

Downloaded from https://academic.oup.com/femsec/article/93/5/fix018/3003318 by guest on 20 April 2024

Table 1. Species composition of cryoconite material (pooled for three cryoconite holes).

Cyanophyta	Chlorophyta	Streptophyta	Chromophyta
Leptolynbya spp.	*Chlamydomonas* cf. *nivalis*	*Ancylonema nordenskiöldii*	Pennate diatom spp.
Nostoc spp.	*Chlamydomonas spp.*	*Cylindrocystis brebissonii*	
Oscillatoria spp.		*Mesotaenium berggrenii*	
Pseudoanabaena spp.			

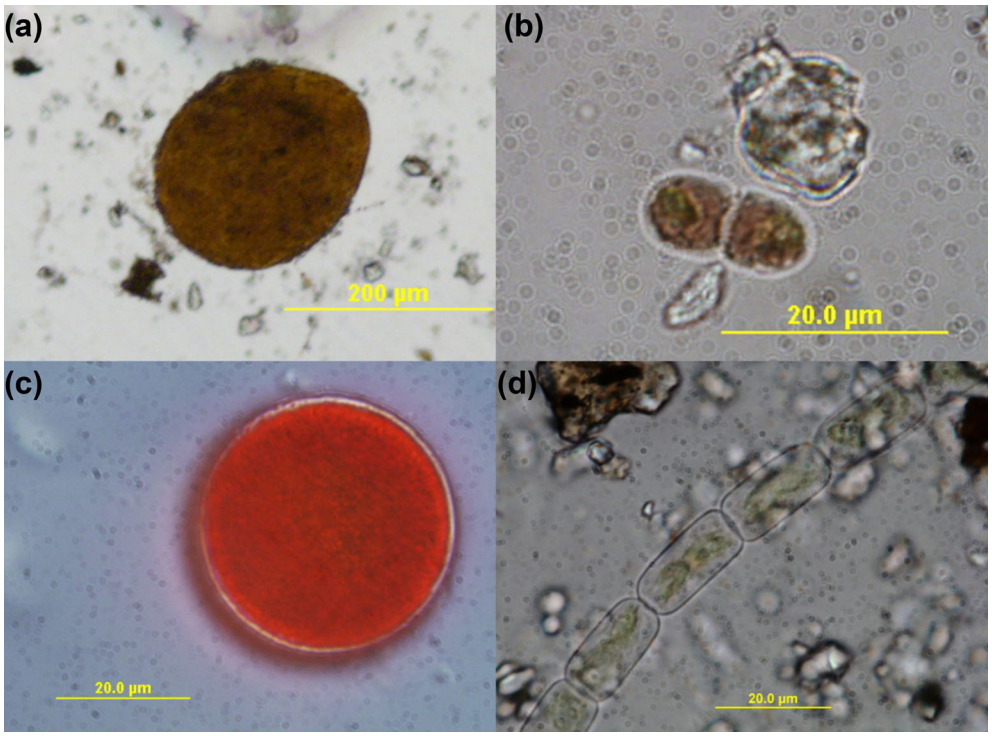

Figure 2. Cyanobacteria and algae from Longyearbreen cryconite: (**a**) *Nostoc* sp. colony; (**b**) dividing cells of *Mesotaenium berggrenii*; (**c**) zygospore of *Chlamydomonas* cf. *nivalis*; (**d**) filament of *Ancylonema nordenskiolldii*.

Community analysis

Cells in cryoconite subsamples were identified using a Leica DM LB2 light microscope with fluorescence attachment. For pigment quantification, subsamples of cryoconite material, frozen (–20°C) were freeze-dried and homogenised prior to the extraction of a known mass (circa 2 g) and pigments were extracted in 100% acetone containing vitamin E as the internal standard. The HPLC protocol was a modified version of the method of Van Heukelem and Thomas (2001), using a c8 column in an Agilent 1100 HPLC equipped with a diode-array detector. Pigments were identified and quantified against analytical standards from DHI and Sigma using both retention time and spectral analysis.

RESULTS

Ambient PAR received on the glacier surface ranged from 200 to 400 μmol m^{-2} s^{-1} (SD 18) during the measurement period. The mean water temperature in the monitored cryoconite hole was 0.9°C, and ranged from 0.4°C to 1.9°C. The sampled holes remained hydrologically connected throughout the monitoring period, although the degree of connection varied diurnally. The sediment layers remained intact; nonetheless, mobile sediment particles were observed moving across the ice surface in the meltwater (Irvine-Fynn, Bridge and Hodson 2011).

Cryoconite phototrophic community composition

Epifluorescence microscopy on cryoconite material revealed the presence of a number of different green algal and cyanobacterial taxa in the three different cryoconite holes sampled (Table 1). Large colonies of *Nostoc* spp. (Fig. 2a) and Streptophytes (closely related to Charophyceae and Embryophyta) were identified in samples from all three holes. Pigments characterising both green algae and cyanobacteria were recorded from the cryoconite material using HPLC (Table 2). Chlorophyll *a* (CHL *a*) pigment dominated all samples, but was higher in hole 1 than holes 2 and 3. Hole 1 also had the highest concentrations of the pigments lutein (LUT), chlorophyll b (CHL b) and echinenone (ECHI)). The ratios of Lutein and CHLb: CHL *a* (Table 3) were two to six times greater than in the other samples, indicating that green algae dominated the community in this hole. There were two key cyanobacterial markers, echinenone (ECHI) and canthaxanthin (CANT), present in all samples from the three cryoconite holes. The orange-brown pigment Scytonemin (present in the sheath of *Nostoc*, Fig. 2a) was found in all samples though it could not be quantified due to poor resolution of the peaks. Although occasional spores of *Chlamydomonas* spp. were found (Fig. 2c), the red pigment astaxanthin was below the detection limit in pigment extracts. Detectable levels of fucoxanthinin holes 1 and 3 indicated that diatoms were also present. Differences in the ratios of pigment markers between holes indicated differences in

Downloaded from https://academic.oup.com/femsec/article/93/5/fix018/3003318 by guest on 20 April 2024

Table 2. Concentration of pigments quantified in by HPLC. Values are given as $\mu g\ g^{-1}$ freeze-dried cryoconite material.

	Hole 1	Hole 2	Hole 3
FUCO (Fucoxanthin)	0.0464	0.0000	0.0513
NEOX (Neoxanthin)	0.0917	0.0000	0.0227
VX (Violaxanthin)	0.1180	0.0141	0.0408
DDX (Diadinoxanthin)	0.0602	0.0275	0.0250
ZX (Zeaxanthin)	0.0543	0.0000	0.0000
LUT (Lutein)	0.6769	0.0176	0.0635
CANT (Canthaxanthin)	0.4924	1.1182	0.6538
CHLB (Chlorophyll b)	1.3474	0.4198	0.0801
ECHI (Echinenone)	0.6267	0.1702	0.2387
CHLA (Chlorophyll a)	10.6670	6.1472	5.4459
CART (Carotenoids)	0.3431	0.0000	0.0622

Table 3. Pigment ratios relative to Chlorophyll a. For abbreviations, see Table 2.

	Site 1	Site 2	Site 3
FUCO	0.0044	0.0000	0.0094
NEOX	0.0086	0.0000	0.0042
VX	0.0111	0.0023	0.0075
DDX	0.0056	0.0045	0.0046
ZX	0.0051	0.0000	0.0000
LUT	0.0635	0.0029	0.0117
CANT	0.0462	0.1819	0.1200
CHLB	0.1263	0.0683	0.0147
ECHI	0.0588	0.0277	0.0438
CART	0.0322	0.0000	0.0114

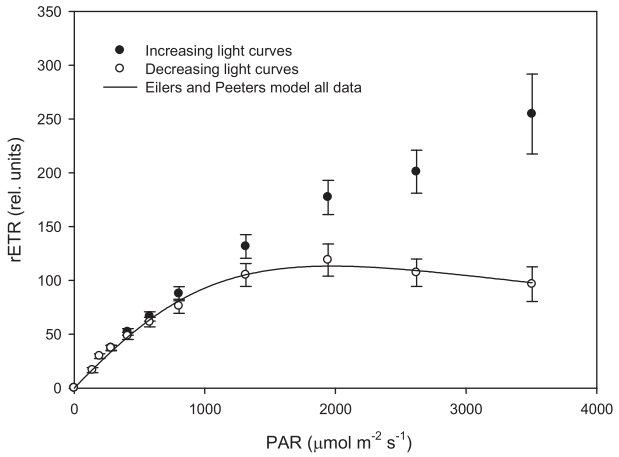

Figure 3. Increasing RLC data (closed symbols, mean ± s.e., $n = 15$) showing no saturation in comparison with decreasing RLC data (open symbols, mean ± s.e., $n = 15$) showing saturated light curves. Fitted line is the Eilers and Peeters (1988) model regressed to the 15 replicate curves data points. Increasing and decreasing light curves were carried out on separate samples each time and with sequentially increasing or decreasing light levels steps, respectively.

relative abundance of taxa, with relatively more cyanobacteria in hole 1.

Cryoconite phototrophic community photophysiology

Increasing RLCs showed virtually no saturation (Fig. 3), with 14 of 15 curves failing to saturate, and one single curve approaching saturation. As a result, $rETR_{max}$ could only be estimated as the highest value obtained (255 ± 37.2 rel. units). In contrast,

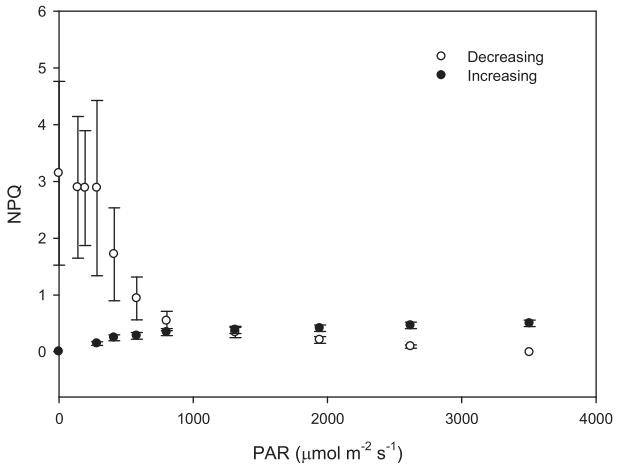

Figure 4. Increasing RLC NPQ data (closed symbols, mean ± s.e., $n = 15$) and decreasing RLC NPQ data (open symbols, mean ± s.e., $n = 15$) for the light curves shown in Fig. 3. Increasing and decreasing light curves were carried out on separate samples each time and with sequentially increasing or decreasing light levels steps, respectively.

decreasing RLCs (Fig. 3) showed clear saturation, with all 15 curves saturating and an $rETR_{max}$ of 113 rel. units ($F_{2,10} = 551$, $p<0.001$). Hence, $rETR_{max}$ determined from decreasing RLCs was <50% of the value estimated from the non-saturating, increasing RLCs. Examination of both sets of RLCs showed no significant difference in the light saturation coefficient (α), with values of 0.13 (increasing) and 0.12 (decreasing) rel. units. For decreasing RLCs, an E_k of 940 and E_s of 1800 $\mu mol\ m^{-2}\ s^{-1}$ PAR were determined.

Calculated downregulation in the form of non-photochemical quenching (NPQ) was notably different between increasing and decreasing RLCs (Fig. 4); note that calculated values do not correct for NPQ retained from the period prior to measurements, i.e. induced under ambient light. For decreasing RLCs, there was no initial dark light curve step, and hence no reversal of any NPQ that had been induced under ambient light prior to the measurement period. Whilst NPQ slowly increased with PAR from 0 to 0.50 ± 0.06 during increasing RLCs, an inverse relationship between NPQ and PAR was apparent during decreasing curves: as light levels were stepped down from 3505 to ~800 $\mu mol\ m^{-2}\ s^{-1}$ PAR, NPQ slowly increased. With further reductions in PAR, NPQ rapidly increased to approximately six times that induced during increasing RLCs. These high levels of NPQ were further retained in the dark during the final 30-s step of decreasing RLCs.

Examination of RLC fluorescence yields revealed the dynamics underlying observed differences in downregulation between increasing and decreasing RLCs (Fig. 5). During increasing RLCs (Fig. 5a), initial increases in both F and F_m' signified reversal of NPQ retained from illumination of samples by ambient light prior to measurements: such retained NPQ was reversed under the initially low PAR levels of increasing RLCs. As samples were subjected to increasing light intensity, F_m' decreased steadily to 84 ± 23.2% of initial values due to NPQ induction, whilst F' returned to approximately initial values (103 ± 29.3% of the value in the dark). Conversely, both F' and F_m' slowly decreased below initial values (measured in the dark, F_o and F_m) at the beginning of decreasing RLCs (Fig. 5b), with decreases accelerating at light intensity <ca. 800 $\mu mol\ m^{-2}\ s^{-1}$, the point at which NPQ increased. With decreases in light intensity to 140 $\mu mol\ m^{-2}\ s^{-1}$, F' reduced to 53 ± 9.9% and F_m' to 64 ± 11.4% of initial values. Note

Downloaded from https://academic.oup.com/femsec/article/93/5/fix018/3003318 by guest on 20 April 2024

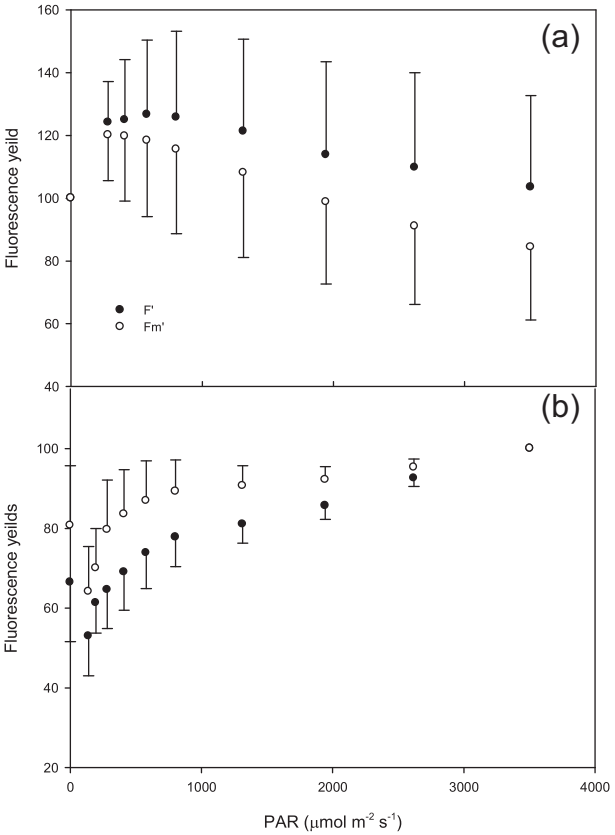

Figure 5. Operational fluorescence yield (F', closed symbols) and maximum fluorescence yield (F_m', open symbols) yield for increasing (**a**) and decreasing (**b**) RLCs shown in Fig. 1 (both data sets mean ± s.e., $n = 15$). Data are represented as the percentage of the initial values obtained from the first light curve step in each case (hence 100% at 0 μmol m^{-2} s^{-1} for increasing and 100% at 3600 μmol m^{-2} s^{-1} PAR for decreasing light curve steps).

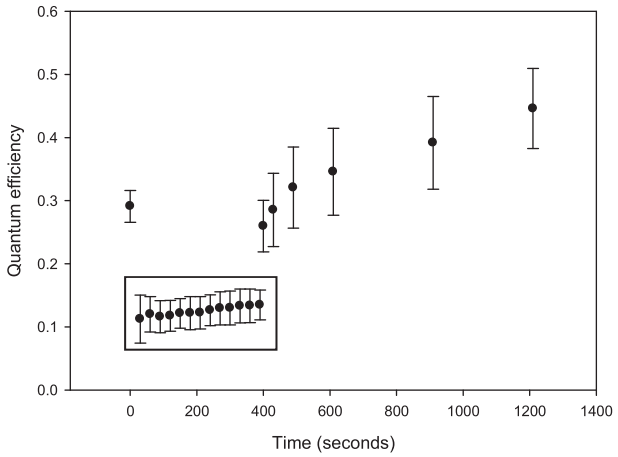

Figure 6. Quantum efficiency during induction–recovery curve measurements (mean ± s.e., $n = 8$). The boxed area shows the efficiency during the induction phase with applied actinic light, other data points are in darkness.

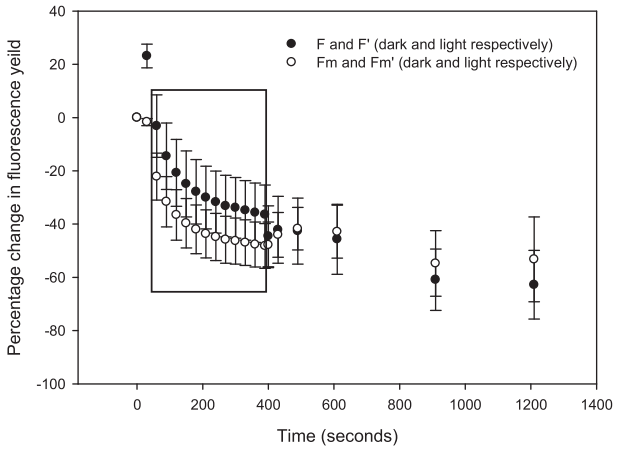

Figure 7. Percentage change, relative to initial values, of the operational fluorescence yield (F and F' in the dark and light respectively) and maximum fluorescence yield (F_m and F_m' respectively) during induction–recovery curves (mean ± s.e., $n = 8$). The boxed area shows the yields measured during the induction phase with applied actinic light, other data points are in darkness.

the slight increase in both F' and F_m' when exposed to darkness at the end of decreasing RLCs (Fig. 5b).

Monitoring of photochemistry during induction–recovery curves indicated a small amount of photoacclimation during the 400-s induction phase at 803 μmol m^{-2} s^{-1}, whereby initial declines in quantum efficiency from 0.29 ± 0.025 to 0.11 ± 0.038 at the onset of illumination were recovered to 0.13 ± 0.025 by the end illumination (Fig. 6). With the onset of the dark recovery phase, rapid increases in quantum efficiency to 0.26 ± 0.041 demonstrated almost full recovery to initial values. During the remainder of the recovery phase, quantum efficiency slowly increased to 0.45 ± 0.063, i.e. well above initial values, suggesting significant retention of downregulation in samples from exposure to ambient light prior to measurements. However, examination of the operational (F' or F in the induction and recovery phases, respectively) and maximum (F_m' or F_m, respectively) fluorescence yields (Fig. 7) revealed unexpected patterns. F' initially increased during the induction phase, presumably due to ubiquinone Qa reduction (lack of increase in F_m' precluding NPQ relaxation), before decreasing as Qa oxidation (unlikely) and/or NPQ induction (most likely) occurred during the induction phase. After 400 s, decreases in F with the onset of the dark recovery phase, presumably reflecting Qa oxidation, outweighed the effects of NPQ reversal; however, continued decreases in F over the remainder of the recovery phase suggested continued NPQ induction in darkness. In a similar manner, F_m' decreased during the induction phase suggesting NPQ induction showed a slight increase with the onset of the recovery phase, i.e. slight NPQ reversal, though subsequently declined over the remainder of the recovery phase indicating continued NPQ induction in the dark. Increases in quantum efficiency during the recovery phase (Fig. 6) were the result of a greater proportional decrease in F compared to F_m (Fig. 7).

DISCUSSION

Cryoconite phototrophs on Longyearbreen, Svalbard, demonstrated a high capability for rapid photoacclimation, via a combination of behavioural and physiological downregulation of photochemistry. The former involves a self-shading process, either chloroplast shading, cell positioning within the cryoconite sediment, or both processes. The latter appears to be a combination of two forms of NPQ; however, this is complicated as a result of the mixed community due to employment of state changes by cyanobacteria which induce rapid changes in fluorescence yields in the same form as NPQ. Overall, there is a high plasticity of photoacclimation in croconite phototrophs, which

Downloaded from https://academic.oup.com/femsec/article/93/5/fix018/3003318 by guest on 20 April 2024

ensures that cells are ideally adapted to high light exposure on the ice surfaces in these high-stress polar environments.

The phototrophic communities of the three cryoconite holes investigated clearly differed despite being hydrologically connected. Pigment analysis indicated that all three holes showed the typical dominance of green algae and cyanophyta within cryoconite material (Langford, Hodson and Banwart 2011; Cameron, Hodson and Osborn 2012; Yallop *et al.* 2012; Edwards *et al.* 2014), with only trace levels of fucoxanthin and hence low biomass of diatoms. Hole 1 was dominated by green algae, principally chlorophytes and streptophytes (indicated by high Chl b: Chl a ratio and the relatively high presence of lutein; streptophytes are closely related to Charophyceae and Embryophyta and hence have similar pigments), whereas holes 2 and 3 were relatively more dominated by cyanobacteria. The cyanobacteria community also differed between holes, based on the relative concentrations of echinenone and canthaxanthin, although all three holes had a high relative abundance of *Nostoc*. Interestingly, there were no significant differences in community measurements of photophysiology between the holes, despite the differences in phototrophic community structure.

Photophysiological data from RLCs and induction–recovery curves demonstrated a high plasticity of response, with several mechanisms of photoacclimation identified that allow the cryoconite phototrophic community to effectively photoacclimate to the high-light regime experienced *in situ*. Photoacclimation methods can be considered to be either physiological or behavioural (Perkins *et al.* 2002, 2010a,b; Lavaud and Goss 2014). Physiological photoacclimation refers largely to photochemical downregulation, including NPQ in eukaryote phototrophs, whereby the light-driven de-epoxidation of specific xanthophyll pigments quenches excess excitation energy in the antennae complex as heat (Consalvey *et al.* 2005; Lavaud and Lepetit 2013). In cyanobacteria, state transitions to balance excitation between photosystems is also a form of physiological photochemical regulation (Campbell *et al.* 1998). Behavioural photoacclimation is largely cell motility as a response to changes in light environment, whereby cells move away from high light or towards low light in order to optimise their efficiency of photochemistry (Forster and Kromkamp 2004; Perkins *et al.* 2002, 2010a,b). However, Yallop *et al.* (2012) expanded upon this by hypothesising that ice algae used chloroplast movement to facilitate shading behind dark, tertiary pigments. Separation of the two processes through *in situ* measurements would be extremely difficult, if not impossible; hence, we refer to behavioural downregulation as the likely composite of these two processes. We therefore hypothesise that cryoconite phototrophs utilise chloroplast movement and/or cell positioning in order to adjust to changing light environments. Such cell motility to facilitate shading within the cryoconite matrix likely explains why light curves with increasing light increments failed to saturate, whereas decreasing light curves did saturate. Increasing curves provide enough time for chloroplast movement inside the cells and/or cell or filament movement in the sediment and hence the cells optimise their light environment. Phototrophic cryoconite communities are organised around granule structures, consisting of mineral grains, microorganisms and polymers (Takeuchi, Kohshima and Seko 2001; Hodson *et al.* 2010; Langford *et al.* 2010; Segawa *et al.* 2014). This is analogous to microbial biofilms in fine sediments, where downregulation is achieved using a mixture of cell motility and NPQ (Perkins *et al.* 2010a,b; Lavaud and Goss 2014). In these systems, a lack of RLC saturation has been attributed to cell movement away from increasing light levels (Perkins *et al.* 2002, 2010a,b). Cyanobacteria, green algae and diatoms are known to utilise cell motility to move away from high light and UV stress through the process of microcycling and bulk migration (Bebout and Garcia-Pichel 1995; Kromkamp, Barranguet and Peene 1998; Perkins *et al.* 2002, 2010a,b; Consalvey *et al.* 2004; Forster and Kromkamp 2004; Serôdio 2004). During this study, microscopy and pigment profiles confirmed the presence of cyanobacteria, diatoms (at very low levels of abundance) and green algae in the cryoconite material, corroborating previous findings (Stibal *et al.* 2006; Yallop and Anesio 2010), and hence supporting the potential of cell motility as a means of downregulation. Cell movement within sediment is usually facilitated by EPS production (Consalvey *et al.* 2004), which is a well-reported characteristic of cryoconite granules (Langford *et al.* 2010; Zarsky *et al.* 2013; Segawa *et al.* 2014). Granules promote community stability (Hodson *et al.* 2010; Irvine-Fynn, Bridge and Hodson 2011; Langford *et al.* 2014; Bagshaw *et al.* 2016b) and, as we now reveal, also play a role in behavioural photoacclimation, Aggregation of cryoconite into granules thus enhances community production, by supporting a stable, cooperative microbial community, enabling physical migration to cope with the extreme glacier surface environment.

Behavioural downregulation of photochemistry (chloroplast movement and/or cell positioning within the sediment) has therefore been demonstrated for cryoconite phototrophic communities, but what is the role of physiological downregulation (in the form of NPQ in green algae and diatoms and state transitions in cyanobacteria) for these phototrophs? Calculation of NPQ from the change in maximum fluorescence yield during increasing incremental RLCs indicated an initial reversal of NPQ retained from exposure to ambient light prior to measurements, highlighting NPQ as an important mechanism of downregulation employed by cryoconite communities *in situ*. The subsequent slow induction of NPQ to values of around 0.5 during increasing RLCs further suggested this form of downregulation to be applied proportionally to irradiance, as is a commonly held assumption underlying NPQ dynamics in microalgae (e.g. Lavaud and Goss 2014). However, by extending our assessment to include both decreasing light curves and induction–recovery curves, we were able to demonstrate unique features in the dynamics of cryoconite community downregulation that would not have been ascertainable using the commonly applied increasing light curve technique alone. First, contrasting dynamics in downregulation during increasing and decreasing light curves indicated that behavioural, as opposed to physiological, downregulation may form the major photoacclimation mechanism employed in cryoconite holes on Svalbard glaciers. This would be in agreement for observations on sediment biofilm communities in intertidal estuaries (Perkins *et al.* 2010a,b; Cartaxana *et al.* 2011). This is evidenced by the 6-fold higher induction of NPQ apparent during decreasing as compared to increasing light curves, although the true magnitude difference in NPQ induction should not be directly compared, due to the differential levels of cell movement hypothesised. Cell movement to induce shading would result in a decrease in F_m' yield as well as that observed due to induction of NPQ (Forster and Kromkamp 2004; Perkins *et al.* 2010a,b), thus confounding the measurement of NPQ based on change in maximum fluorescence yield (see Methods). Thus, high NPQ could in fact be the sum of true NPQ induction and cell movement both reducing F_m' yield. However, it is highly likely that the observed patterns in NPQ are indeed primarily physiological downregulation (energy-dependent downregulation in eukaryote microalgae, but also state transitions in cyanobacteria, see below), at least in decreasing RLCs due to the timing and rate of induction.

Downloaded from https://academic.oup.com/femsec/article/93/5/fix018/3003318 by guest on 20 April 2024

As well as demonstrating the significantly higher capacity for NPQ available to cryoconite phototrophs than estimated from increasing light curves, these trends provide insight into the likely balance between behavioural and physiological downregulation employed *in situ*. During increasing light curves, it is likely that chloroplast movement and/or cell positioning in the sediment matrix, i.e. behavioural downregulation, reduced the light stress experienced by cells, therefore reducing the requirement to induce NPQ. In contrast, the initial high light stress experienced during decreasing curves, coupled with the lack of time for chloroplast movement and/or cell positioning, resulted in cells inducing physiological downregulation, i.e. NPQ, as a means to balance the irradiance provided. By comparing the magnitude of NPQ induced with/without the presence of behavioural downregulation, data indicate that the latter may account for ca. 75% of the total downregulation employed in cryoconite holes. In eukaryote microalgae, this may be an adaptation to reduce the metabolic costs associated with production and interconversion of NPQ-associated pigments (Lavaud and Goss 2014) in this high-light environment. Second, the contrasting dynamics in downregulation observed during this study strongly indicated that additional to a combination of behavioural and typical physiological forms of downregulation, the cryoconite phototrophic communities further possess a rapidly induced, time or light-dose-dependent form of NPQ, as opposed to primarily light intensity-driven forms. With the onset of decreasing light curves, an initial slow level of NPQ was induced, followed by a more rapid induction at light levels below 800 μmol m^{-2} s^{-1} PAR. This would parallel the different forms of NPQ reported for diatoms (Lavaud and Goss 2014), although diatoms were observed to have extremely low abundance in the cryoconite. Rapidly induced energy-dependent downregulation of this form which is not reversed in darkness has been reported (Lavaud and Lepetit 2013) and referred to as photoinhibitory quenching (qI) or saturating NPQ (NPQs). NPQ was induced rapidly during our experiment, despite decreasing light levels, and was also retained in the dark. Such trends were also apparent during the dark recovery phase of induction–recovery curves. Examination of the fluorescence yields showed that both F and F_m initially increased in the dark recovery phase, presumably due to NPQ reversal, but then declined despite the increase in dark quantum efficiency (F_v/F_m) observed. There would therefore appear to be either a time or potentially light-dose-dependent form of physiological downregulation that, once triggered, does not decrease with decreasing PAR, nor is rapidly (i.e. within the duration of dark recovery employed here) reversed in the dark.

It is important to note that our measurements were made on a mixed community largely dominated by green algae and cyanobacteria. The latter appear not to have energy dependent NPQ but rapid changes in fluorescence are observed through state transitions utilising phycobilosome diffusion (Campbell and Öquist 1996; Campbell *et al.* 1998). This form of rapid downregulation would result in similar changes in fluorescent yields as NPQ in green algae, e.g. a quenching as light increased followed by reversal in darkness. During increasing RLCs, state transitions (state 2 to state 1) would result in a decrease in F_m' and hence an increase in our measured NPQ; however, shading processes through cell motility described above would negate the need for this downregulation in increasing RLCs. In decreasing light curves, state 2 to state 1 transition would be induced in cyanobacteria at the same time as energy-dependent NPQ would be induced in the eukaryote microalgae. It may be that as light levels reduced in these decreasing RLCs, the induction of this state transition was not reversed increasing the relative level of quenching and hence the large increase in measured NPQ. Obviously, it would not be possible to differentiate between the two processes in such a mixed community using *in situ* fluorescence measurements; however, we suggest that there is a high likelihood of physiological downregulation employed by both the eukaryote microalgae (energy-dependent downregulation) and cyanobacteria (state transitions).

The combination of chloroplast movement, cell positioning and physiological downregulation by the cryoconite phototrophs is a highly efficient method of light acclimation that has serious implications for the interpretation of fluorescence-based assessments of productivity. Specifically, the lack of saturation of light curves with increasing light increments indicates caution is required when utilising fluorescence on cryoconite. Productivity ($rETR_{max}$) can clearly be significantly overestimated when photoacclimation during the light curve occurs, whether this is through cell movement or chloroplast shading. In this study, the first steps of the RLC appear to be relatively unaffected, with α similar for increasing and decreasing RLCs. However, as the light curves progressed, divergence between the curves showed an overestimation of $rETR_{max}$ of over 100%, with similar overestimation likely for light saturation parameters E_s and E_k. This should be corrected for in studies using fluorescence in order to avoid overestimation of productivity, and potentially the role of cryoconite phototrophs in carbon flux calculations (Hodson *et al.* 2007; Anesio *et al.* 2010; Cook *et al.* 2012; Chandler *et al.* 2015; Bagshaw *et al.* 2016a).

In conclusion, this study demonstrates that the phototrophic cryoconite community on Longyearbreen, Svalbard, utilises a mixture of behavioural and physiological (likely a mixture of NPQ in eukaryotes and state transitions in cyanobacteria) downregulation of photochemistry. Cells appear to be capable of optimising their light environment through chloroplast shading and/or cell positioning within the cryoconite, effectively behavioural downregulation. Shading through chloroplast movement and cell positioning is likely to result in an overestimation of productivity when using increasing incremental RLCs. In future work, this may be corrected for by using the product of ETR and the operational fluorescence F' (Ihnken *et al.* 2014); however, this was tested in this study and did not alter the shape of the RLCs. In the cryoconite studied here, the phototrophs, primarily a mixture of green algae and two different cyanophyte communities, showed high plasticity of photophysiology, indicating extremely high capability for light acclimation. This would be expected for cells inhabiting polar ice surfaces, where light intensity and light dose can be high and fluctuate quickly. Aggregation of cryoconite into granules is therefore an important adaptation which not only prolongs microbial community stability, but also allows light acclimation and hence promotes ecosystem productivity.

ACKNOWLEDGEMENTS

We should also like to thank the two anonymous reviewers for their highly constructive reviews.

FUNDING

RP was funded by a British Phycological Society Small Project Grant. LM had combined funding from Royal Geography Society Small Research Grant, Geological Society of London Robert Scott Memorial Award and Forskningsradet Norge, Arctic Field Grant no 246072. The work was carried out on Research Project RiS

Downloaded from https://academic.oup.com/femsec/article/93/5/fix018/3003318 by guest on 20 April 2024

10281. MLY was supported by a Leverhulme Research Fellowship RF 2014–708.

Conflict of interest. None declared.

REFERENCES

Anesio AM, Sattler B, Foreman CM *et al.* Carbon fluxes through bacterial communities on glacier surfaces. *Ann Glaciol* 2010;**51**:32–40.

Bagshaw EA, Tranter M, Fountain AG *et al.* Do cryoconite holes have the potential to be significant sources of C, N, and P to downstream depauperate. *Arct Antarct Alp Res* 2013;**45**: 440–54.

Bagshaw EA, Tranter M, Wadham JL *et al.* Dynamic behaviour of supraglacial lakes on cold polar glaciers: Canada Glacier, Mcmurdo Dry Valleys, Antarctica. *J Glaciol* 2010;**56**:366–8.

Bagshaw EA, Tranter M, Wadham J *et al.* Processes controlling carbon cycling in Antarctic glacier surface ecosystems. *Geochem Persp Lett* 2016a; v2 n1 doi: 10.7185/geochemiet.1605.

Bagshaw EA, Wadham JL, Tranter M *et al.* Response of Antarctic Cryoconite microbial communities to light. *FEMS Microbiol Ecol* 2016b; **92**, doi: 10.1093/femsec/fiw076.

Bebout BM, Garcia-Pichel F. UVB-induced vertical migrations of cyanobacteria in a microbial mat. *Appl Environ Microb* 1995;**61**:4215–22.

Benning LG, Anesio AM, Lutz S *et al.* Biological Impact on Greenland's Albedo. *Nat Geosci* 2014;**7**:691.

Campbell D, Hurry V, Clarke AK *et al.* Chlorophyll fluorescence analysis of cyanobacterial photosynthesis and acclimation. *Microbiol Mol Biol R* 1998:**62**:667–83

Campbell D, Öquist G. Predicting light acclimation in Cyanobacteria from nonphotochemical quenching of photosystem II fluorescence, which reflects state transitions in these organisms. *Plant Physiol* 1996;**111**:1293–8.

Cameron KA, Hodson AJ, Osborn AM. Structure and diversity of bacterial, eukaryotic and archaeal communities in glacial cryoconite holes from the Arctic and the Antarctic. *FEMS Microbiol Ecol* 2012;**82**:254–67.

Cartaxana P, Ruivo M, Hubas C *et al.* Light and O2 microenvironments in two contratsing diatom-dominated coastal sediments. *Mar Ecol Prog Ser* 2011;**545**:35–47

Chandler DM, Alcock JD, Wadham JL *et al.* Seasonal changes of ice surface characteristics and productivity in the ablation zone of the Greenland ice sheet. *Cryosphere* 2015; **9**:487–504.

Consalvey MC, Jesus B, Perkins RG *et al.* Monitoring migration and measuring biomass in benthic biofilms: the effects of dark/far-red adaptation and vertical migration on fluorescence measurements. *Photosynth Res* 2004;**81**:91–101

Consalvey MC, Perkins RG, Paterson DM *et al.* PAM fluorescence: a beginners guide for benthic diatomists. *Diatom Res* 2005;**20**: 1–22

Cook JM, Hodson AJ, Anesio AM *et al.* An improved estimate of microbially mediated carbon fluxes from the Greenland ice sheet. *J Glaciol* 2012;**58**:1098–108.

Dieser M, Greenwood M, Foreman CM. Carotenoid pigmentation in Antarctic heterotrophic bacteria as a strategy to withstand environmental stresses. *Arctic Antarc Alp Res* 2010;**42**:396–405.

Edwards A, Mur LAJ, Girdwood SE *et al.* Coupled cryoconite ecosystem structure-function relationships are revealed by comparing bacterial communities in Alpine and Arctic glaciers. *FEMS Microbiol Ecol* 2014;**89**:222–37.

Eilers PHC, Peeters JCH. A model for the relationship between light intensity and the rate of photosynthesis in phytoplankton. *Ecol Model* 1988;**42**:199–215.

Etzelmüller B, Schuler TV, Isaksen K *et al.* Modeling the temperature evolution of Svalbard permafrost during the 20th and 21st century. *Cryosphere* 2011;**5**:67–79.

Forster RM, Kromkamp JC. Modelling the effects of chlorophyll fluorescence from subsurface layers on photosynthetic efficiency measurement in microphytobenthic algae. *Mar Ecol-Prog Ser* 2004;**284**:9–22

Foreman CM, Wolf CF, Priscu JC. Impact of episodic warming events on the physical, chemical and biological relationships of lakes in the Mcmurdo Dry Valleys, Antarctica. *Aquat Geochem* 2004;**10**:239–68.

Hammer Ø, Harper DAT, Ryan PD. PAST: Paleontological Statistics Software Package for Education and Data Analysis. *Palaeontol Electron* 2001;**4**:9.

Hodson A, Anesio AM, Ng F *et al.* A glacier respires: quantifying the distribution and respiration Co2 flux of cryoconite across an entire Arctic supraglacial ecosystem. *J Geophys Res-Biogeo* 2007;**112**, doi: G04s3610.1029/2007jg000452.

Hodson A, Cameron K, Boggild C *et al.* The structure, biological activity and biogeochemistry of cryoconite aggregates upon an Arctic Valley Glacier: Longyearbreen, Svalbard. *J Glaciol* 2010;**56**:349–62

Ihnken S, Kromkamp J, Beardall J *et al.* State-transitions facilitate robust quantum yields and cause an over-estimation of electron transport in Dunaliella tertiolecta cells held at the CO2 compensation point and re-supplied with DIC. *Photosynth Res* 2014;**119**:257–72.

Irvine-Fynn TDL, Bridge JW, Hodson AJ. In situ quantification of supraglacial cryoconite morphodynamics using time-lapse imaging: an example from Svalbard. *J Glaciol* 2011;**57**:651–7.

Kaczmarek L, Jakubowska N, Celewicz-Goldyn S *et al.* The microorganisms of cryoconite holes (Algae, Archaea, Bacteria, Cyanobacteria, Fungi, and Protista): a review. *Polar Rec* 2016;**52**:176–203.

Kromkamp J, Barranguet C, Peene J. Determination of microphytobenthos PSII quantum efficiency and photosynthetic activity by means of variable chlorophyll fluorescence. *Mar Ecol Prog Ser* 1998;**162**:45–55

Larsson S. Geomorphological effects on the slopes of Longyear Valley, Spitsbergen, after a heavy rainstorm in July 1972. *Geogr Ann A* 1982;**64**:105–25.

Langford HJ, Hodson A, Banwart S *et al.* The microstructure and biogeochemistry of Arctic cryoconite granules. *Ann Glaciol* 2010;**51**:87–94.

Langford HJ, Hodson A, Banwart S. Using Ftir spectroscopy to characterise the soil mineralogy and geochemistry of cryoconite from Aldegondabreen Glacier, Svalbard. *Appl Geochem* 2011;**26**:S206–9.

Langford HJ, Irvine-Fynn TDL, Edwards A *et al.* A spatial investigation of the environmental controls over cryoconite aggregation on Longyearbreen Glacier, Svalbard. *Biogeosciences* 2014;**11**:5365–80.

Lavaud J, Goss R. The peculiar features of non-photochemical fluorescence quenching in diatoms and brown algae. In Non-Photochemical Quenching and Energy Dissipation in Plants, Algae and Cyanobacteria Netherlands: Springer. 2014 (pp. 421–43).

Lavaud J, Lepetit B. An explanation for the inter-species variability of the photoprotective and non-photochemical chlorophyll fluorescence quenching in diatoms. *Biochim Biophys Acta* 2013;**1827**:294–302

Downloaded from https://academic.oup.com/femsec/article/93/5/fix018/3003318 by guest on 20 April 2024

Lawson EC, Wadham JL, Tranter M *et al*. Greenland ice sheet exports labile organic carbon to the Arctic Oceans. *Biogeosciences* 2014;**11**:4015–28.

Lutz S, Anesio AM, Villar SEJ *et al*. Variations of algal communities cause darkening of a Greenland glacier. *FEMS Microbiol Ecol* 2014;**89**:402–14.

McMinn A, Ryan KG, Ralph P *et al*. Spring sea ice photosynthesis, primary productivity and biomass distribution in eastern Antarctica, 2002–2004. *Mar Biol* 2007;**151**:985–995

Musilova M, Tranter M, Bamber JL *et al*. Experimental evidence that microbial activity lowers the albedo of glaciers. *Geochem Persp Lett* 2016;**2**:106–16; doi: http://dx.doi.org/10.7185/geochemlet.1611.

Perkins RG, Kromkamp JC, Serôdio J *et al*. The application of variable chlorophyll fluorescence to microphytobenthic biofilms. In Suggett D, Prasil O, Borowitzka M (eds) *Chlorophyll a Fluorescence in Aquatic Sciences: Methods and Applications: Developments in Applied Phycology*, **vol. 4**. 2010a, 237–75. Springer, UK.

Perkins RG, Lavaud J, Serôdio J *et al*. Vertical cell movement is a primary response of intertidal benthic biofilms to increasing light dose. *Mar Ecol Prog Ser* 2010b;**16**:93–103

Perkins RG, Mouget J-L, Lefebvre S *et al*. Light response curve methodology and possible implications in the application of chlorophyll fluorescence to benthic diatoms. *Mar Biol* 2006;**149**:703–12.

Perkins RG, Oxborough K, Hanlon ARM *et al*. Can chlorophyll fluorescence be used to estimate the rate of photosynthetic electron transport within microphytobenthic biofilms? Mar. *Ecol Prog Ser* 2002;**228**:47–56

Remias D, Pichrtová M, Pangratz M *et al*. Secondary pigments and ultrastructure of Chlainomonas sp. (Chlorophyta) from the European alps compared with Chlamydomonas vivalis forming red snow. *FEMS Microbiol Ecol* 2016;**92**, doi:10.1093/femsec/fiw030

Segawa T, Ishii S, Ohte N *et al*. The nitrogen cycle in cryoconites: naturally occurring nitrification-denitrification granules on a glacier. *Environ Microbiol* 2014;**16**:3250–62.

Serôdio J. Analysis of variable chlorophyll fluorescence in microphytobenthos assemblages: implications of the use of depth-integrated measurements. *Aquat Microb Ecol* 2004; **36**:137–52

Stibal M, Elster J, Šabacká M *et al*. Seasonal and diel changes in photosynthetic activity of the snow alga Chlamydomonas nivalis (Chlorophyceae) from Svalbard determined by pulse amplitude modulation fluorometry. *FEMS Microbiol Ecol* 2007;**59**:265–73.

Stibal M, Sabacka M, Kastovska K. Microbial communities on glacier surfaces in Svalbard: impact of physical and chemical properties on abundance and structure of cyanobacteria and algae. *Microb Ecol* 2006;**52**:644–54.

Takeuchi N. Optical characteristics of cryoconite (surface dust) on glaciers: the relationship between light absorbency and the property of organic matter contained in the cryoconite. *Ann Glaciol* 2002a;**32**:409–14.

Takeuchi N. Surface albedo and characteristics of cryoconite (biogenic dust) on an Alaskan Glacier, Gulkana in the Alaska range. *Bull Glaciol Res* 2002b;**19**:63–70.

Takeuchi N, Kohshima S, Seko K. Structure, formation, and darkening process of albedo-reducing material (Cryoconite) on a Himalayan Glacier: a granular algal mat growing on the glacier. *Arct Antarc Alp Res* 2001;**33**:115–22.

Tedesco M, Doherty S, Fettweis X *et al*. The darkening of the Greenland ice sheet: trends, drivers, and projections (1981-2100). *Cryosphere* 2016;**10**:477–96.

Van Heukelem L, Thomas CS. Computer-assisted high-performance liquid chromatography method development with applications to the isolation and analysis of phytoplankton pigments. *J Chromatogr A* 2001; 910:31–49

Yallop ML, Anesio AM. Benthic diatom flora in supraglacial habitats: a generic-level comparison. *Ann Glaciol* 2010;**51**:15–22.

Yallop ML, Anesio AM, Perkins RG *et al*. Photophysiology and albedo-changing potential of the ice algal community on the surface of the Greenland ice sheet. *Isme Journal* 2012;**6**: 2302–13.

Zarsky JD, Stibal M, Hodson A *et al*. Large cryoconite aggregates on a Svalbard glacier support a diverse microbial community including ammonia-oxidizing Archaea. *Environ Res Lett* 2013;**8**, doi:10.1088/1748-9326/8/3/035044

Zawierucha K, Kolicka M, Takeuchi N *et al*. What animals can live in cryoconite holes? A faunal review. *J Zool* 2015;**295**:159–69.

Downloaded from https://academic.oup.com/femsec/article/93/5/fix018/3003318 by guest on 20 April 2024